

# Do earthquakes “know” how big they will be? a neural-net aided study

Neri Berman,<sup>1,2,\*</sup> Oleg Zlydenko,<sup>2</sup> Oren Gilon,<sup>2</sup> Yossi Matias,<sup>2</sup> and Yohai Bar-Sinai<sup>1,†</sup>

<sup>1</sup>*School of Physics, Tel-Aviv University*

<sup>2</sup>*Google Research*

Earthquake occurrence is notoriously difficult to predict. While some aspects of their spatiotemporal statistics can be relatively well captured by point-process models, very little is known regarding the magnitude of future events, and it is deeply debated whether it is possible to predict the magnitude of an earthquake before it starts. This is due both to the lack of information about fault conditions and to the inherent complexity of rupture dynamics. Consequently, even state of the art forecasting models typically assume no knowledge about the magnitude of future events besides the time-independent Gutenberg Richter (GR) distribution, which describes the marginal distribution over large regions and long times. This approach implicitly assumes that earthquake magnitudes are independent of previous seismicity and are identically distributed. In this work we challenge this view by showing that information about the magnitude of an upcoming earthquake can be directly extracted from the seismic history. We present MAGNET - MAGNitude Neural EsTimation model, an open-source, geophysically-inspired neural-network model for probabilistic forecasting of future magnitudes from cataloged properties: hypocenter locations, occurrence times and magnitudes of past earthquakes. Our history-dependent model outperforms stationary and quasi-stationary state of the art GR-based benchmarks, in real catalogs in Southern California, Japan and New-Zealand. This demonstrates that earthquake catalogs contain information about the magnitude of future earthquakes, prior to their occurrence. We conclude by proposing methods to apply the model in characterization of the preparatory phase of earthquakes, and in operational hazard alert and earthquake forecasting systems.

## I. INTRODUCTION

Earthquakes are notoriously unpredictable, and forecasting seismicity is a long-standing scientific and technological challenge, often deemed unrealistic due to the inherent complexity of earthquake processes and the scarcity of near-field data [1, 2]. Research since the late 19th century has provided much phenomenological insight about the spatiotemporal statistics of earthquakes, including various marginal distributions [3, 4], scaling relations [5–8] and characteristics of both spatial and temporal clustering [9–13]. Clearly, these insights can be used to quantitatively inform us about future seismicity based on recent history. For example, Omori’s law tells us that after big earthquakes we should expect an increase in the local seismicity rate [9]. Such laws have been incorporated into a variety of forecasting models, which are operationally used today [14–17].

However, these statistical relations only describe the rate and locations of earthquakes, and very little is known about the dependence of earthquake magnitude on seismic history. It is deeply debated whether it is possible to determine the magnitude of an earthquake before it starts [4, 18], or even during rupture [19, 20]. Most modeling approaches assume that event magnitudes follow an identical and independent stationary (or almost stationary) distribution - the Gutenberg Richter distribution (GR), which describes the marginal magnitude distribution over large regions and long times. While some

variations in magnitude statistics have been described [21, 22], they all model history dependence by weak and slow changes in the parameters of the GR distribution, and do not model the magnitude of a *specific* future event. Operationally, state-of-the-art forecasting models typically assume no knowledge about the magnitude of future events besides the marginal GR distribution, an assumption known as separability [23]. Namely, the separability assumption is that the distribution of earthquake magnitudes is statistically independent of their locations and times.

This modeling approach is not a naive or uninformed choice. Current research on magnitude prediction has failed to show a universal and reproducible advantage over a stationary or quasi-stationary GR benchmark [18, 24]. Indeed, due to the spatial complexity of the elastic fields, faulting patterns and lithology, the nonlinearities of the rupture process and the complicated interaction between them all, it is not far-fetched to assume that determining the magnitude of an event requires a detailed microscopic knowledge of the system’s state. This philosophy also inspired physical models which describe earthquake dynamics with a statistical approach [5, 25–27]. These models reproduce many of the phenomenological statistical relations by positing that faults evolve (“self-organize”) towards a critical state, where events emerge stochastically. The magnitudes then follow a power-law distribution which is scale-free and self-similar, akin to physical systems in the vicinity of a phase transition. Under this paradigm, determining the magnitude of an event is indeed impossible using only far-field measurements.

Multiple previous studies have not identified a defini-

---

\* [neriberman@gmail.com](mailto:neriberman@gmail.com)

† [ybarsinai@gmail.com](mailto:ybarsinai@gmail.com)

tive link between earthquake magnitude and seismic history [28–30]. Some studies have shown circumstantial evidence that earthquake magnitudes may not follow a strictly stationary distribution, e.g. by showing that statistics are not invariant to permutation of the order, or by showing that the maximal magnitude in a given time frame can be predicted with a better-than-random chance [31–38]. However, a significant information gain over the GR benchmark in predicting the magnitude of a given earthquake was not demonstrated. The debate regarding the dependence of magnitude on seismic history remains open.

The main goal of this paper is to ask the question directly: can we extract any information about the magnitude of a specific future earthquake from regional seismic history? A positive answer would have two important consequences. From a fundamental point of view, it challenges the common belief that earthquake magnitudes are inherently unpredictable. Second, it suggests that the separability assumption, which is widely applied in operational earthquake forecasting, may be replaced by a more nuanced model that incorporates the seismic history into the magnitude prediction. This may lead to improved forecasting models, and potentially also be used to identify precursory signals in the seismic history of an earthquake.

To this end, we construct MAGnitE Neural EsTimation model, MAGNET, a neural-based model that predicts the magnitude of a given earthquake given the short and long term seismic history prior to its occurrence. Our model is trained on seismic catalogs containing information about past earthquakes, including location, time, and magnitude. In some experiments, we also incorporate focal mechanism information. Importantly, the model is not tasked with predicting the timing and location of the event, as they are explicitly provided. Thus, we separate out the task of modeling nucleation statistics and isolate the question of magnitude predictability. If our model performs better than a draw from the GR distribution or its variants, as we will indeed demonstrate is the case, we assert that at least some information about the magnitude of a specific earthquake is extractable from cataloged properties alone. An example of MAGNET’s performance on a few select earthquakes is shown in Fig 1a. For instance, MAGNET improved the likelihood of estimating the true magnitude for the Ridgecrest mainshock in Southern California and the Kaikōura event in New Zealand by factors of approximately 13 and 4, respectively, over the naive GR predictor.

## II. METHODOLOGY

MAGNET is a generative neural network (NN) that takes as input a hypocentral catalog of regional seismicity, and the time and location of a future event (a “query”). The network produces a probability density function (PDF) estimating its magnitude.

MAGNET is composed of two main components. First, the catalog up to time  $t$  (excluding  $t$ ) is encoded by a series of geophysically inspired functions and long-short term memory (LSTM) units, which produces a latent representation of the seismic history [39]. Second, this representation is combined with a space-time query specifying the coordinates,  $\mathbf{x}_i, t_i$ , of a future earthquake and passed into a fully connected neural network (FCNN) that produces a parametrized PDF of the event’s magnitude,  $p_{\mathbf{x}_i, t_i}(m)$ , see Fig. 1a.

Technically, the distribution is modeled as a mixture of two stretched Kumaraswamy distributions [40] and is parameterized by 5 parameters, which are the output of the network. This parameteric family can smoothly interpolate between a power-law decaying distribution (resembling the GR distribution), and localized distributions with concentrated mass around a specific value. This allows the model to output both an “ignorant” prediction, essentially resembling the GR distribution, and more confident predictions localized around a given magnitude.

The model parameters are optimized to maximize the log likelihood (LL) of the observed magnitudes. Importantly, during training we only supply the model with queries about spacetime coordinates where earthquakes indeed occurred, and only events above the completeness magnitude of the catalog are used as queries. A detailed description of the model’s architecture is given in the methods section.

We applied MAGNET on three distinct earthquake catalogs to assess the performance across diverse seismogenic regions: the Hauksson Catalog [41] for Southern California, GeoNet [42] for New Zealand, and the JMA catalog [43] for Japan. While all three catalogs encompass highly active seismic zones, they are compiled using various measurement methodologies and exhibit varying data quality. A separate model is trained for each region, with identical loss function and parameterization of the PDF. All metrics reported in this work were evaluated over a time span that is not included in the training period.

The resulting PDF is presented in Fig. 1b for a few examples of major events, superimposed on the stationary GR distribution (fitted on the train set), which is the naive benchmark. It can be seen that for most presented earthquakes, the likelihood of the observed magnitude is higher for MAGNET than for the GR benchmark, and in some cases MAGNET’s prediction differs qualitatively as well as quantitatively. The presented metrics demonstrate that our model consistently and significantly outperforms all benchmarks across all test regions, indicating a significant information gain in forecasting earthquake magnitudes prior to their occurrence.

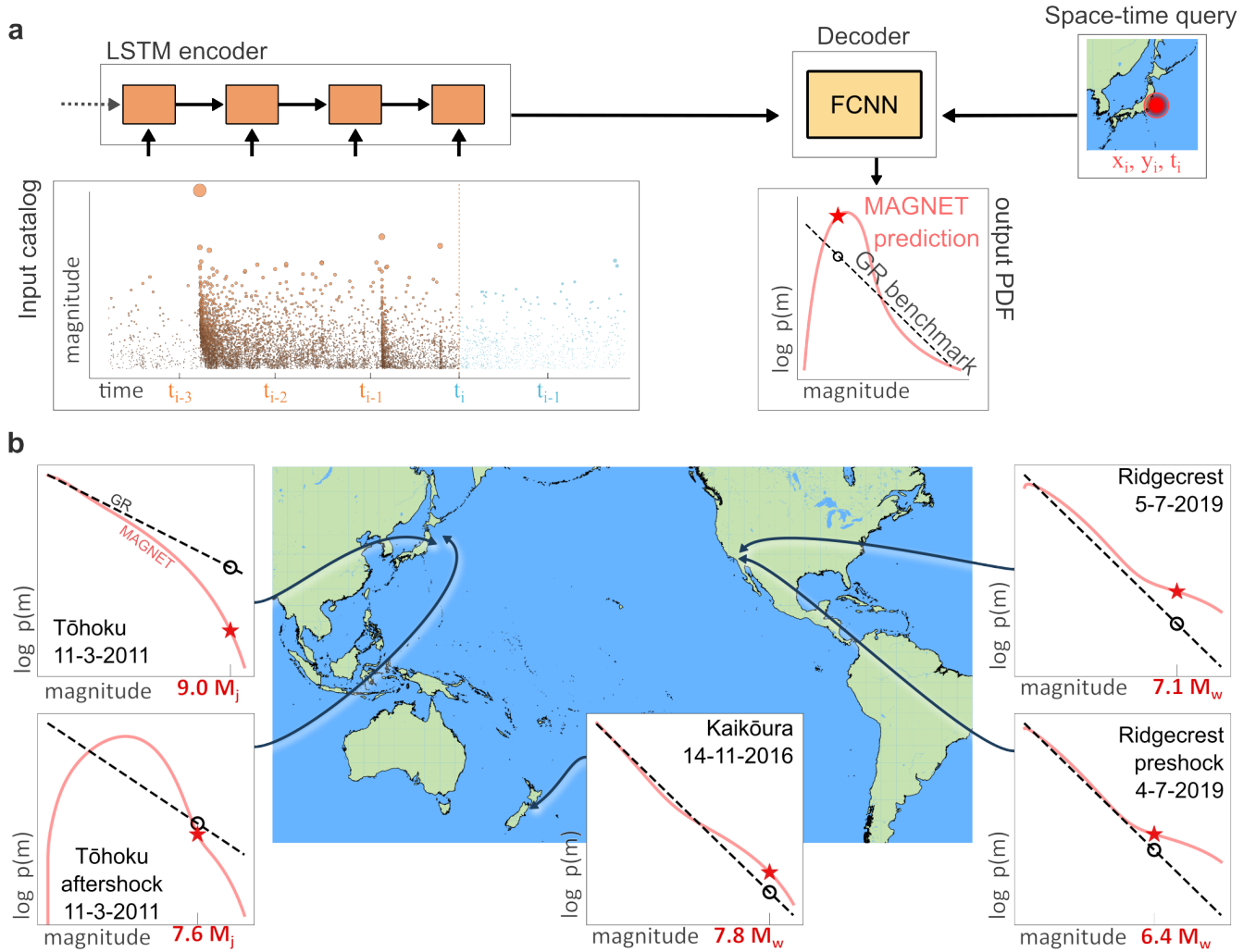


FIG. 1. **a** MAGNitude Neural EsTimation model (MAGNET) task and architecture. Seismic history is continuously encoded using a Long Short-Term Memory neural network. For each earthquake, the encoded history up to its occurrence time ( $t_i$ ) is concatenated with the time and location of the earthquake (“space - time query”). The combined information is fed into a fully-connected neural network that outputs a probability density function (PDF) of the predicted magnitude at that time and location. In turn, the output is compared to a benchmark model (e.g. GR in dashed line) **b** Performance on major earthquakes: MAGNET’s resulting PDFs for a selection of well-known major earthquakes worldwide. The red curve represents the model’s predicted PDF and the dashed black curve represents the Gutenberg-Richter (GR) magnitude-frequency distribution, a common naive benchmark. For most earthquakes shown here, the likelihood of the observed magnitude (red star) is higher for MAGNET than for the GR benchmark (black circle). Notably, the Tōhoku aftershock shows a qualitatively different behavior.

### III. RESULTS

As explained above, the model outputs a PDF  $p_{\mathbf{x}_i, t_i}(m_i)$  for each earthquake in the test set. We denote by  $\ell_i$  the log-likelihood of the observed magnitude  $m_i$  as predicted by MAGNET,

$$\mathcal{L} = -\langle \ell_i \rangle, \quad \ell_i = \log(p_{\mathbf{x}_i, t_i}(m_i)) \quad (1)$$

$\mathcal{L}$  is the average minus log-likelihood, which the model is trained to minimize. The values of  $\ell_i$  for MAGNET and the leading benchmark are presented in Extended Material (EM) Fig. 9.

Figure 2a shows the predicted PDFs for 100 randomly sampled events from the Southern California test set. The PDFs exhibit a clear trend: those that were calculated for higher-magnitude events are skewed towards larger magnitudes (warmer colors) compared to lower-magnitude events (cooler colors). This aligns with the expected behavior for an earthquake magnitude predictor. For comparison, the stationary GR distribution, the naive predictor which is independent of (recent) seismic history, is presented along the model’s results.

This is a qualitative demonstration that the model works as expected. For a quantitative comparison, we calculate  $\mathcal{L} = -\langle \ell_i \rangle$  over all events in the test set, and benchmark it against state-of-the-art models: the stationary Gutenberg-Richter (GR) distribution (fitted over the training set), and a few variants of a moving window GR approach [21]. It is seen that MAGNET significantly and consistently outperforms all benchmarks across all three regions, as shown in Fig. 3a-c. Further comparison to other benchmarks is given in Table I.

In addition to comparing the log-likelihood of the observed data, one can convert the prediction problem to a binary question: will the earthquake at the spacetime query  $\mathbf{x}_i, t_i$  have a higher magnitude than a threshold  $m_t$ ? This can be easily calculated from the prediction, as the probability that  $m_i > m_t$  is simply  $\int_{m_t}^{\infty} p(m') dm'$ . This task, asking whether a given event will be a large earthquake, is more interpretable and can be evaluated using standard binary classification metrics such as area under the receiver operator (ROC) curve [44] and under the interpolated precision-recall (PR) curve [45]. Fig. 3d-f and g-i show these metrics for all three regions examined and compare against the GR-variant models. Again, MAGNET outperforms all benchmarks.

Finally, Figure 2b presents the marginal probability density function (PDF) of magnitudes for MAGNET’s prediction,  $P(m) = N^{-1} \sum_i p_{\mathbf{x}_i, t_i}(m)$ . This represents the average probability distribution of magnitudes over the whole test set. It is seen that although the model was not constrained to do so, the average distribution aligns well with the “uninformed” GR distribution. That is, although MAGNET’s prediction for each individual earthquake may deviate significantly from the GR distribution, it does reproduce this well known long-time behavior on average. It is also seen that the average prediction of the 300-event moving window GR deviates

significantly from the GR distribution. We also observe that MAGNET’s average prediction aligns well with the *test set* GR distribution, rather than the training set, suggesting its ability to generalize beyond the training data. This observation is more pronounced in the New Zealand and Japan data sets presented in Extended Data Fig. 8.

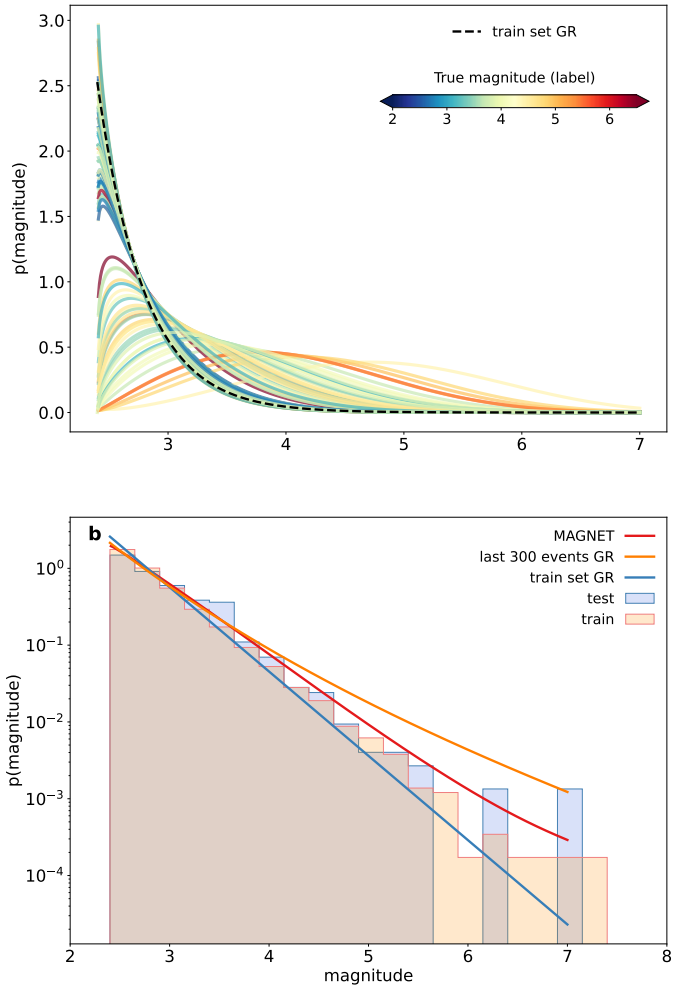


FIG. 2. **MAGNET’s output.** **a**, Predicted magnitude PDFs produced by MAGNET for 100 randomly sampled events from the test set in the Southern California region. Curves are colored according to the magnitude of each earthquake event. It is seen that the PDFs for high magnitude events are generally skewed towards higher magnitudes, as expected from a predictive model. We superimpose the train set Gutenberg-Richter distribution (dashed black line). **b**, Marginal magnitude distribution produced by MAGNET. That is, the average of all PDFs from the test set. It is seen that the marginal distribution closely resembles the GR distribution, though follows the test set distribution more precisely. In addition, we plot a similar marginal PDF for common benchmarks for the entire test set. Histograms of the train (and test) set are presented in orange (blue).

It is interesting to examine MAGNET’s information gain per event, which is quantified by the difference in



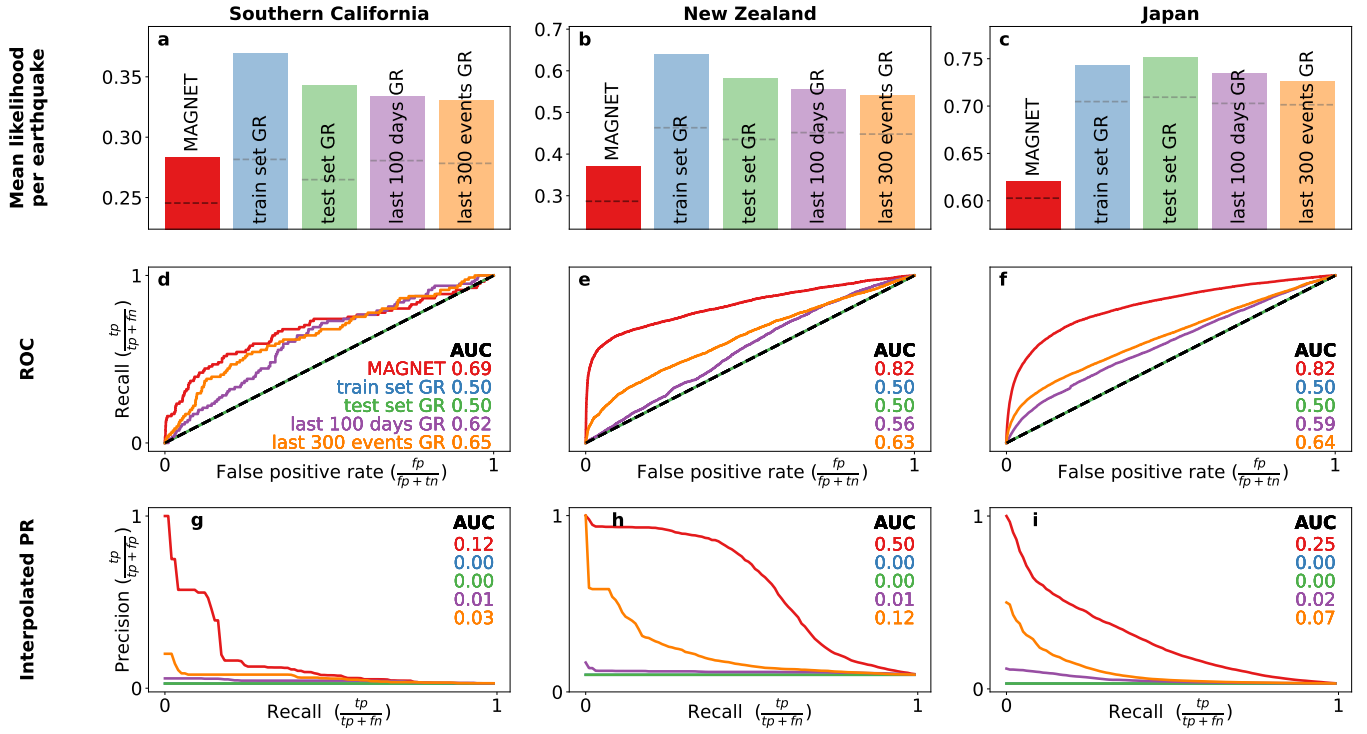


FIG. 3. **Benchmarking MAGNET.** **a, b, c**, Minus mean information content of our MAGNET model (red) and other common benchmark magnitude predictors (see labels on bars in the figure). A lower score indicates a better performing model. Scores conditioned above the temporal incompleteness are marked by the horizontal dashed line on each corresponding bar. **d, e, f**, Receiver Operating Characteristic (ROC) and **g, h, i** the interpolated precision-recall (PR) curve for a binary classifier determining the next event will be large ( $m \geq 4$ ). The performance of such a classifier can be quantified by the area under the curve (AUC), noted in each frame, color coded identically to the bar plots. For the AUC metrics, a higher score indicates a better performing classifier.

Model	$\mathcal{L}$			$\mathcal{L}$ temporally conditioned			$\mathcal{L}$ spatially conditioned		
	Southern California	New Zealand	Japan	Southern California	New Zealand	Japan	Southern California	New Zealand	Japan
MAGNET	<b>0.28</b>	<b>0.37</b>	<b>0.62</b>	<b>0.25</b>	<b>0.29</b>	<b>0.60</b>	<b>0.27</b>	<b>0.31</b>	<b>0.47</b>
train set GR	0.37	0.64	0.74	0.28	0.46	0.70	0.36	0.41	0.51
test set GR	0.34	0.58	0.75	0.26	0.44	0.71	0.33	0.39	0.50
last 300 events GR	0.33	0.54	0.73	0.28	0.45	0.70	0.32	0.38	0.51
last 100 days GR	0.33	0.56	0.73	0.28	0.45	0.70	0.32	0.39	0.53

TABLE I. Mean score,  $\mathcal{L}$ , for various tested benchmarks.  $\mathcal{L}$  is computed by Eq. 1. Lower score indicates a better magnitude predictor, best score in column is indicated in bold. First 3 columns display scores for the raw calculation of  $\mathcal{L}$ , middle and right column triplets display the scores for the temporally and spatially conditioned  $\mathcal{L}$  scores, respectively.

log-likelihood (LL) of the observed magnitude,

$$\Delta\ell_i = \log p_{\mathbf{x}_i, t_i}^{(MAGNET)}(m_i) - \log p^{(GR)}(m_i) \quad (2)$$

Analyzing this quantity per event across the entire test set reveals patterns indicating where and when our model achieves its advantage. Fig. 4a shows the test set for Southern California events magnitudes by their running index, colored according to the information gain as defined in Eq. 2. This time-domain representation allows us to track the cumulative information gain, calculated over the entire test set and displayed as the blue dashed line in the figure. The predominantly increasing trend in cumulative information gain suggests that our model is consistently advantageous as opposed to identifying some local trends such as immediate aftershock sequences. Notably, for the Southern California data set, the most rapid information gain occurs during the aftershocks of the two Ridgecrest earthquakes. Surprisingly, even the pre-shock and main shock events demonstrate positive information gains over the GR benchmark, with  $\Delta\ell$  values of 0.5 and 1.4 nats ( $\log(2)$  nat = 1 bit), respectively.

Our analysis reveals a persistent increase in information gain across the test set for all investigated regions (Fig. 4b-d). Specifically, we show an average information gain of  $> 0.1$  nats per earthquake in the same region in Japan where Ogata et. al. [18] found no information gain. Similar plots for the other studied regions are shown in EM Fig. 6.

#### IV. INTERPRETATION AND POTENTIAL CAVEATS

At this point, it is clear that MAGNET achieves an information gain about the magnitude of specific earthquakes, prior to their occurrence. However, such a gain may potentially result not from the fact that the underlying physical process is predictable (at least to some extent), but from various measurement and modeling artifacts.

One such artifact is “short-time incompleteness” (STI): the fact that immediately following a large event the signal of subsequent small events might be buried in the coda of the mainshock [10, 24]. Thus, immediately after a large event, smaller events are less likely to be included in the catalog, not because they did not occur, but rather because they were not detected. Indeed, our model consistently allocates less probability mass to low magnitudes shortly after large events (see the Tohoku aftershock in Fig. 1b), and some of the information gain may be attributed to this effect.

In order to factor the effect of STI from the information gain calculation, we recalculate the likelihood score of each event,  $p(m_i)$ , conditioned on the magnitude exceeding a threshold,  $\tilde{m}$ , which is the time-dependent completeness magnitude:

$$p(m|m_i > \tilde{m}) = \frac{p_{\mathbf{x}_i, t_i}(m)}{\int_{\tilde{m}}^{\infty} p(m') dm'} \quad (3)$$

The instantaneous completeness magnitude,  $m_c(t)$ , is defined as the minimal magnitude above which all earthquakes can be detected. If we choose  $\tilde{m} \geq m_c$  then, by definition, the model cannot present an information gain due to the STI effect.

We thus take  $\tilde{m} = m_c(t)$ , which we estimate dynamically using the maximum curvature method [46] within a window of 150 past and 150 current and future events. The resulting  $m_c(t)$  curves are presented in the EM Fig. 7. The conditioned cumulative information gain (CIG) is then recalculated and presented as the yellow dashed curved in Fig. 4 for all three tested regions. Indeed, factoring out the temporal incompleteness reduces the information gain, though it is still significant: evidently, the conditioned CIG curves show a steadily increasing trend. The horizontal dashed lines on the bars in Fig 3a-c indicate the mean conditioned scores, also presented in Table II. EM Table I displays the conditioned scores for all benchmarks tested in this study.

Similarly to the temporal domain, a spurious information gain may also be caused by temporally constant but spatially varying statistical properties. For example, fault stresses, geometry and lithology may change in space resulting in a spatially-dependent GR distribution [47–50], and the local completeness magnitude is also generally spatially dependent. In such a case, the information gain of MAGNET does not imply that the magnitudes are correlated in time.

To examine this, we preform two additional tests. First, we construct a spatially dependent GR distribution which accounts for the local variation in seismic statistics. We use the method proposed by [51], as detailed in the Methods section. The spatially dependent GR shows some information gain over plain-vanilla GR in New Zealand and Japan, but not in California, see EM Table II. In any case, this information gain is always smaller than MAGNET’s, with the sole exception of the temporally-conditioned test in New Zealand.

Second, similar to the temporal analysis, we calculate the information gain conditioned on the locally-varying completeness magnitude. Specifically, we use Eq. 3, with a spatially varying completeness  $\tilde{m} = m_c(x, y)$ , estimated for a coordinate grid of  $0.1^\circ$ , see Methods section for details.

The spatially conditioned CIG are shown by the red dashed curves in Fig. 4. It is a steadily increasing function for the Southern California and Japan data sets. In the New Zealand data set the curve shows an initial increase followed by a plateau after the first sequence of major events (the 2016 Te Araroa and Kaikōura earthquakes). This may indicate that a good portion of this information gain followed by these earthquakes does originate from spatially inhomogeneity, as also hinted by the

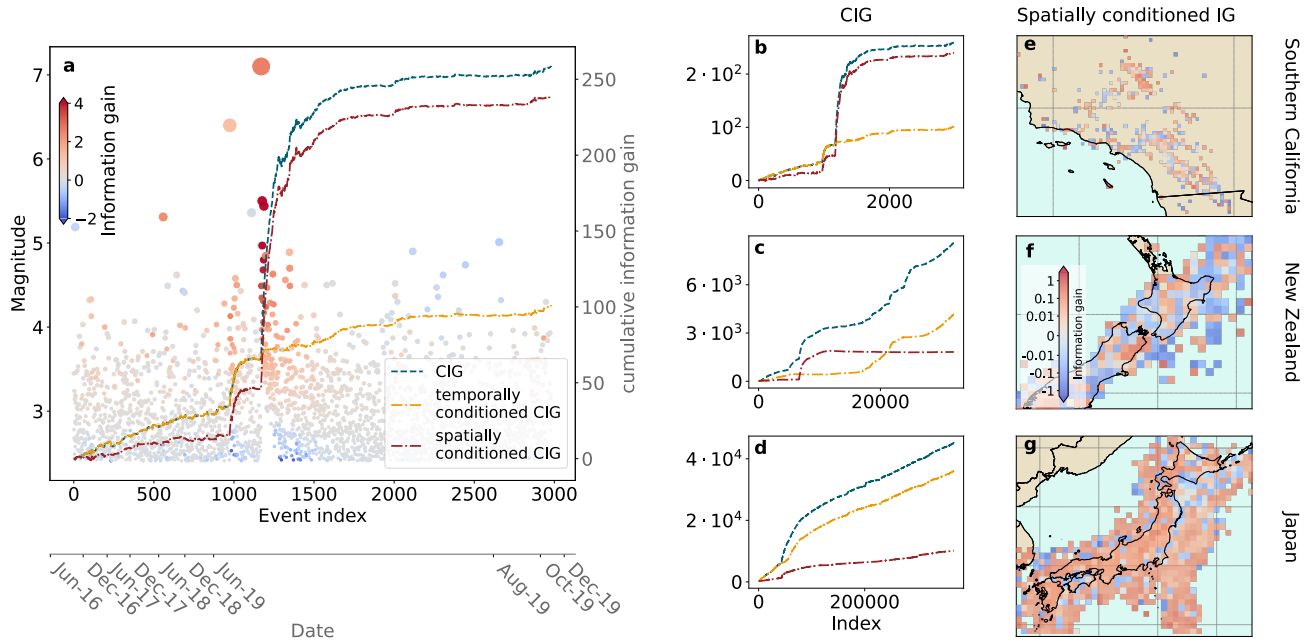


FIG. 4. **Information gain in MAGNET.** **a**, Information gain of individual events in the Southern California test set. Scattered dots indicate magnitude at event index, colored by the information gain per event (scale is indicated by colorbar), here warm is an advantage for MAGNET, while cool is an advantage for the benchmark. Secondary horizontal axis (grey) indicates the corresponding origin time. Cumulative Information gain (CIG) (dashed blue), temporally conditioned CIG (dashed yellow) and spatially conditioned CIG (dashed red) curves are superimposed on the scatter, demonstrating a constantly increasing function. **b-d**, Information gain (dashed blue) and temporally and spatially conditioned CIG (dashed yellow and red respectively) curves for Southern California, New Zealand and Japan test sets, respectively, all three regions examined in this study. An exception from the increasing trend can be observed for the spatially conditioned CIG of New Zealand (red curve in c). **e-g** Spatial distribution of spatially conditioned information gain for all regions in study. Maps show the difference in mean information content per bin, model's advantage is indicated by warm colors, disadvantage by cool colors, as defined by the colorbar adjacent to f.

spatially-varying GR benchmark. Nevertheless, the overall score still shows an advantage for our model over the test set. Fig. 4e-g shows the spatial distribution of MAGNET’s advantage over the GR benchmark. All three regions exhibit a spatially diffuse pattern, suggesting that information is not gained solely from any one specific area (compare EM Fig. 10 for the distribution of seismicity).

## V. IMPLICATIONS AND OUTLOOK

In this work we have used neural based models to find statistical dependencies between earthquake magnitudes and seismic history. Since our model is provided with the known location and timing of an event and is only tasked with predicting its magnitude, we have separated out the question of rate and location of earthquakes, and directly probe whether their magnitude is history dependent. MAGNET shows robust and significant information gain, even after accounting for possible measurement artifacts such as temporal or spatially dependent properties compared against a host of benchmarks, thereby answering an open question in earthquake predictability. Our results indicate that some information about the magnitude of a specific event can be extracted, on average, from the regional seismic history in the form of a hypo-center catalog.

This means that the seismic patterns preceding large events are distinguishable, at least to some extent, from those preceding “background” activity. A similar claim was recently raised by Ben - Zion and Zaliapin[11], which show trends in statistical properties of the seismicity prior to fault-size events, though a direct linkage between the two observation requires further investigation. In general, it would also be interesting to understand what are the statistical features of seismicity that our model identifies, which may be done using various explainability analyses [52–54].

Understanding such patterns will advance the effort of earthquake prediction a great deal[55–59], though it is still further down the road. Additionally, such models may be incorporated in early warning systems, which already provide a quick (though not accurate) estimation of the source time and location. Another possible application is incorporating a history-dependent magnitude distribution into point-process rate forecasting models, such as the epidemic type aftershock sequence model (ETAS) or similar [14, 60, 61]. As discussed above, such models currently assume no statistical dependence of the magnitude. Since larger earthquakes produce more aftershocks, a more accurate estimation of magnitudes will have a positive compounding effect on the resulting statistics.

## VI. METHODS

### A. Neural architecture

A detailed visual of the model’s architecture is presented in Extended Data Fig. 5. The catalog is used as an input into three distinct encoding components:

**Recent Earthquakes Encoder** Calculates a set of predefined (non trainable) functions on various past time windows. The result is then used as input to a LSTM NN. A detailed description of this encoder is given in Zlydenko et. al. [62].

**Seismicity Rate Encoder** Computes a rough estimation of the amount of energy released in a given region around the query coordinate, in a given past time window. The result is then input to a LSTM NN. A detailed description of this encoder is found in Zlydenko et. al. [62].

**Spacetime Query Encoder** Time is represented as the time difference from the most recent past event, in seconds. No further processing is done in this encoder.

Outputs of all encoders are concatenated and fed to a Fully Connected Neural Network (FCNN). The sizes of layers in the FCNN, as the number of layers themselves, are optimized by cross validation. A `tanh` activation is used for the hidden layers, and a `softplus` as an activation on the output layer.

### B. Loss metric

To obtain the Probability Density Function (PDF) of the magnitudes ( $p(m)$ ) for each query coordinates ( $\mathbf{x}_i, t_i$ ) we maximize the likelihood,  $\mathcal{L} = -\langle \ell_i \rangle$ , where  $\langle \cdot \rangle$  is the mean over all examples in the set. The PDF is taken to be a mixture of two stretched and shifted Kumaraswamy distributions [40]:

$$p(m) \equiv \sum_{j=1,2} \left[ \frac{A_j}{\sigma} a_j b_j \left( \frac{m - m_c}{\sigma} \right)^{(a_j - 1)} \left( 1 - \left( \frac{m - m_c}{\sigma} \right)^{a_j} \right)^{(b_j - 1)} \right] \quad (4)$$

Here  $a_j, b_j$  are the parameters of the Kumaraswamy distribution.  $m_c$  is the train set’s completeness magnitude.  $m_c$  together with  $\sigma$  define the support of  $p(m)$  to  $[m_c, m_c + \sigma]$ .  $A_j$  is a normalization prefactor, with  $j$  the summation index defining the PDF mixture.



### C. Definition of benchmark models

**Last  $n$  events** The Gutenberg- Richter (GR) distribution fitted for the past  $n$  events. This method follows Gulia & Wiemer[21] for constructing a b-value time-series. If in the last  $n$  events there are less than 10 earthquakes of magnitudes above  $m_c^{train}$ , then more events from the past are included, until this condition is met.  $m_c^{train}$  is estimated using the maximal curvature method[46].

**Last  $d$  days** The Gutenberg- Richter (GR) distribution fitted for the events in the past  $d$  days. This method is identical to the previous method in all but the definition of the window selection.

**Spatially varying GR** Estimation of the local  $b$  value is done by following the method of Taroni et. al. [51]. Seismicity data is binned into  $0.1^\circ \times 0.1^\circ$  bins, and the GR distribution is fitted for each bin.  $b$  for a specified location  $x_i$  is calculated by the average of all  $b$  values in bins within 30km around  $x_i$ . Estimates which consider less than 150 events are discarded.

**Kernel density estimation (KDE) of last  $n$  events** Selecting the last  $n$  events (similar to described in *last  $n$  events*) we compute the KDE estimation of the magnitude PDF, using the 'scott' estimator bandwidth[63]. This is implemented using the SciPy tool[64]. The resulting PDF is used as the prediction of the magnitude.

### D. Measurement of incompleteness

**Temporal incompleteness** Temporal incompleteness is measured at the times of events by fitting the completeness magnitude to a window of 300 events: 150 past events, 1 current event, 149 future events. The window is constructed by the same algorithm as in the *Last  $n$  events benchmark*.

**Spatial incompleteness** Spatial incompleteness is calculated for a grid of coordinates, spaced by  $\theta^\circ$  degrees, covering the relevant region.  $\theta$  is set to 0.1 for

Southern California and 0.5 for New Zealand and Japan data sets. Calculation is done using train set's events. The value per point is calculated using the maximal curvature method[46], over the nearest, at least 100 events, with a minimal radius of  $\theta^\circ$ . In cases where the nearest 100 events span over a radius of  $2^\circ$  the data point is considered invalid. Events from the test set are divided into bins of  $\theta^\circ$  centered around the point for which  $m_c(x, y)$  was computed. Events are assigned with the  $m_c$  value of their bin.

### DATA AND CODE AVAILABILITY

The datasets analysed during the current study are available in the relevant references mentioned throughout the article. The code for analysing the data is available in **\*\*TBA\*\***

Country borders in this work are plotted using data from <https://geojson-maps.kyd.au/>.

### ACKNOWLEDGEMENTS

We thank Yehuda Ben-Zion, Assaf Inbal, Kelian Dascher-Cousineau, David Marsan, Eugenio Lippiello, Jiancang Zhuang and Yosihiko Ogata. for thoughtful discussions. YBS is supported by ISF grant 1907/22 and by Google Gift grant.

### AUTHOR CONTRIBUTIONS

N.B., O.Z., O.G., Y.M. and Y.B.S. designed the research. N.B. conducted the experiments. N.B., O.G. and Y.B.S. performed the statistical analysis. N.B. and O.Z. wrote the code base. N.B. and Y.B.S. wrote the manuscript. All authors reviewed the manuscript.

### AUTHOR INFORMATION

The authors declare no competing interests. Please contact Yohai Bar-Sinai [ybarsinai@gmail.com](mailto:ybarsinai@gmail.com) or Neri Berman [neriberman@gmail.com](mailto:neriberman@gmail.com) for correspondence and requests, including questions regarding reprints and permissions.

- 
- [1] P. Bernard, Earthquake precursors and crustal 'transients', *Nature*, 1 (1999).
  - [2] R. J. Geller, D. D. Jackson, Y. Y. Kagan, and F. Mulargia, Earthquakes Cannot Be Predicted, *Science* **275**, 1616 (1997).
  - [3] B. Gutenberg and C. F. Richter, Frequency of earthquakes in California\*, *Bulletin of the Seismological Society of America* **34**, 185 (1944).
  - [4] Y. Y. Kagan, Seismic moment distribution revisited: I. Statistical results, *Geophysical Journal International* **148**, 520 (2002).
  - [5] P. Bak and C. Tang, Earthquakes as a self-organized critical phenomenon, *Journal of Geophysical Research: Solid Earth* **94**, 15635 (1989).
  - [6] K. Dascher-Cousineau, E. E. Brodsky, T. Lay, and T. H. W. Goebel, What Controls Variations in After-shock Productivity?, *Journal of Geophysical Research*:

- Solid Earth* **125**, e2019JB018111 (2020).
- [7] Y. Y. Kagan, Aftershock Zone Scaling, *Bulletin of the Seismological Society of America* **92**, 641 (2002).
- [8] T. Utsu, Y. Ogata, R. S. S, and Matsu'ura, The Centenary of the Omori Formula for a Decay Law of Aftershock Activity, *Journal of Physics of the Earth* **43**, 1 (1995).
- [9] F. Omori, On After-Shocks of Earthquakes, *Journal of the College of Science, Imperial University of Tokyo* , 111 (1894).
- [10] Y. Y. Kagan, Short-Term Properties of Earthquake Catalogs and Models of Earthquake Source, *Bulletin of the Seismological Society of America* **94**, 1207 (2004).
- [11] Y. Ben-Zion and I. Zaliapin, Localization and coalescence of seismicity before large earthquakes, *Geophysical Journal International* **223**, 561 (2020).
- [12] P. M. R. DeVries, F. Viégas, M. Wattenberg, and B. J. Meade, Deep learning of aftershock patterns following large earthquakes, *Nature* **560**, 632 (2018).
- [13] G. C. P. King, R. S. Stein, and J. Lin, Static stress changes and the triggering of earthquakes, *Bulletin of the Seismological Society of America* **84**, 935 (1994).
- [14] Y. Ogata, Statistical Models for Earthquake Occurrences and Residual Analysis for Point Processes, *Source: Journal of the American Statistical Association* **83**, 9 (1988).
- [15] J. L. Hardebeck, A. L. Llenos, A. J. Michael, M. T. Page, M. Schneider, and N. J. van der Elst, Aftershock Forecasting, *Annual Review of Earth and Planetary Sciences* **52**, null (2024).
- [16] T. H. Jordan, Y. T. Chen, P. Gasparini, R. Madariaga, I. Main, W. Marzocchi, G. Papadopoulos, G. Sobolev, K. Yamaoka, and J. Zschau, OPERATIONAL EARTHQUAKE FORECASTING. State of Knowledge and Guidelines for Utilization, *Annals of Geophysics* **54**, 319 (2011).
- [17] M. Stirling, G. McVerry, M. Gerstenberger, N. Litchfield, R. Van Dissen, K. Berryman, P. Barnes, L. Wallace, P. Villamor, R. Langridge, G. Lamarche, S. Nodder, M. Reyners, B. Bradley, D. Rhoades, W. Smith, A. Nicol, J. Pettinga, K. Clark, and K. Jacobs, National Seismic Hazard Model for New Zealand: 2010 Update, *Bulletin of the Seismological Society of America* **102**, 1514 (2012).
- [18] Y. Ogata, K. Katsura, H. Tsuruoka, and N. Hirata, Exploring Magnitude Forecasting of the Next Earthquake, *Seismological Research Letters* **89**, 1298 (2018).
- [19] W. L. Ellsworth and G. C. Beroza, Seismic Evidence for an Earthquake Nucleation Phase, *Science* **268**, 851 (12.5.95).
- [20] M.-A. Meier, T. Heaton, and J. Clinton, Evidence for universal earthquake rupture initiation behavior: Universal Earthquake Rupture Initiation, *Geophysical Research Letters* **43**, 7991 (2016).
- [21] L. Gulia and S. Wiemer, Real-time discrimination of earthquake foreshocks and aftershocks, *Nature* **574**, 193 (2019).
- [22] S. Nandan, G. Ouillon, and D. Sornette, Magnitude of Earthquakes Controls the Size Distribution of Their Triggered Events, *Journal of Geophysical Research: Solid Earth* **124**, 2762 (2019).
- [23] F. P. Schoenberg, Testing Separability in Spatial-Temporal Marked Point Processes, *Biometrics* **60**, 471 (2004), 3695775.
- [24] S. Stockman, D. J. Lawson, and M. J. Werner, Forecasting the 2016–2017 Central Apennines Earthquake Sequence With a Neural Point Process, *Earth's Future* **11**, e2023EF003777 (2023).
- [25] Z. Olami, H. J. S. Feder, and K. Christensen, Self-organized criticality in a continuous, nonconservative cellular automaton modeling earthquakes, *Physical Review Letters* **68**, 1244 (1992).
- [26] A. Sornette and D. Sornette, Self-Organized Criticality and Earthquakes, *Europhysics Letters* **9**, 197 (1989).
- [27] T. W. J. de Geus and M. Wyart, Scaling theory for the statistics of slip at frictional interfaces, *Physical Review E* **106**, 065001 (2022).
- [28] G. Petrillo and J. Zhuang, Verifying the Magnitude Dependence in Earthquake Occurrence, *Physical Review Letters* **131**, 154101 (2023).
- [29] M. Taroni, Are the magnitudes of earthquakes in Southern California, with incompleteness removed, correlated?, *Geophysical Journal International* **236**, 1596 (2024).
- [30] J. Davidsen and A. Green, Are Earthquake Magnitudes Clustered?, *Physical Review Letters* **106**, 108502 (2011).
- [31] Q. Xiong, M. R. Brudzinski, D. Gossett, Q. Lin, and J. C. Hampton, Seismic magnitude clustering is prevalent in field and laboratory catalogs, *Nature Communications* **14**, 2056 (2023).
- [32] Á. Corral, Comment on “Do Earthquakes Exhibit Self-Organized Criticality?”, *Physical Review Letters* **95**, 159801 (2005).
- [33] I. Spassiani and G. Sebastiani, Exploring the relationship between the magnitudes of seismic events, *Journal of Geophysical Research: Solid Earth* **121**, 903 (2016).
- [34] E. Lippiello, L. de Arcangelis, and C. Godano, A positive answer on the existence of correlations between positive earthquake magnitude differences (2024), arXiv:2404.15706 [physics].
- [35] E. Lippiello, L. de Arcangelis, and C. Godano, A positive answer on the existence of correlations between positive earthquake magnitude differences (2024), arXiv:2404.15706 [physics].
- [36] E. Lippiello, L. de Arcangelis, and C. Godano, Influence of Time and Space Correlations on Earthquake Magnitude, *Physical Review Letters* **100**, 038501 (2008).
- [37] R. Shcherbakov, J. Zhuang, G. Zöller, and Y. Ogata, Forecasting the magnitude of the largest expected earthquake, *Nature Communications* **10**, 4051 (2019).
- [38] A. Panakkat and H. Adeli, NEURAL NETWORK MODELS FOR EARTHQUAKE MAGNITUDE PREDICTION USING MULTIPLE SEISMICITY INDICATORS, *International Journal of Neural Systems* **17**, 13 (2007).
- [39] S. Hochreiter and J. Schmidhuber, Long Short-Term Memory, *Neural Computation* **9**, 1735 (1997).
- [40] P. Kumaraswamy, A generalized probability density function for double-bounded random processes, *Journal of Hydrology* **46**, 79 (1980).
- [41] E. Hauksson, W. Yang, and P. M. Shearer, Waveform Relocated Earthquake Catalog for Southern California (1981 to June 2011), *Bulletin of the Seismological Society of America* **102**, 2239 (2012).
- [42] GNS, *GeoNet Aotearoa New Zealand Earthquake Catalogue* (1970).
- [43] Japan Meteorological Agency website, [https://www.data.jma.go.jp/svd/eqev/data/bulletin/hypo\\_e.html](https://www.data.jma.go.jp/svd/eqev/data/bulletin/hypo_e.html).
- [44] K. P. Murphy, *Machine Learning: A Probabilistic Perspective* (2012).

- [45] S. Büttcher, C. L. A. Clarke, and G. V. Cormack, *Information Retrieval: Implementing and Evaluating Search Engines* (MIT Press, 2010).
- [46] S. Wiemer and M. Wyss, Minimum Magnitude of Completeness in Earthquake Catalogs: Examples from Alaska, the Western United States, and Japan, *Bulletin of the Seismological Society of America* **90**, 859 (2000).
- [47] D. Amitrano, Brittle-ductile transition and associated seismicity: Experimental and numerical studies and relationship with the b value, *Journal of Geophysical Research: Solid Earth* **108**, 10.1029/2001JB000680 (2003).
- [48] C. H. Scholz, On the stress dependence of the earthquake b value, *Geophysical Research Letters* **42**, 1399 (2015).
- [49] M. Herrmann, E. Piegari, and W. Marzocchi, Revealing the spatiotemporal complexity of the magnitude distribution and b-value during an earthquake sequence, *Nature Communications* **13**, 5087 (2022).
- [50] M. Taroni and M. M. C. Carafa, Earthquake size distributions are slightly different in compression vs extension, *Communications Earth & Environment* **4**, 1 (2023).
- [51] M. Taroni, J. Zhuang, and W. Marzocchi, High-Definition Mapping of the Gutenberg–Richter b-Value and Its Relevance: A Case Study in Italy, *Seismological Research Letters* **92**, 3778 (2021).
- [52] P. Sturmfels, S. Lundberg, and S.-I. Lee, Visualizing the Impact of Feature Attribution Baselines, *Distill* **5**, e22 (2020).
- [53] Y. Zhang, P. Tiño, A. Leonardis, and K. Tang, A Survey on Neural Network Interpretability, *IEEE Transactions on Emerging Topics in Computational Intelligence* **5**, 726 (2021).
- [54] Z. Liu and F. Xu, Interpretable neural networks: Principles and applications, *Frontiers in Artificial Intelligence* **6**, 10.3389/frai.2023.974295 (2023).
- [55] S. M. Mousavi and G. C. Beroza, Deep-learning seismology, *Science* **377**, eabm4470 (2022).
- [56] S. M. Mousavi and G. C. Beroza, Machine Learning in Earthquake Seismology, *Annual Review of Earth and Planetary Sciences* **51**, 105 (2023).
- [57] A. Mignan and M. Broccardo, Neural Network Applications in Earthquake Prediction (1994–2019): Meta-Analytic and Statistical Insights on Their Limitations, *Seismological Research Letters* **91**, 2330 (2020).
- [58] S. Karimpouli, D. Caus, H. Grover, P. Martínez-Garzón, M. Bohnhoff, G. C. Beroza, G. Dresen, T. Goebel, T. Weigel, and G. Kwiatek, Explainable machine learning for labquake prediction using catalog-driven features, *Earth and Planetary Science Letters* **622**, 118383 (2023).
- [59] K. J. Bergen, P. A. Johnson, M. V. de Hoop, and G. C. Beroza, Machine learning for data-driven discovery in solid Earth geoscience, *Science* **363**, eaau0323 (2019).
- [60] Y. Ogata, Statistics of Earthquake Activity: Models and Methods for Earthquake Predictability Studies, *Annual Review of Earth and Planetary Sciences* **45**, 497 (2017).
- [61] K. Dascher-Cousineau, O. Shchur, E. E. Brodsky, and S. Gunnemann, Using Deep Learning for Flexible and Scalable Earthquake Forecasting, *Geophysical Research Letters* **50**, e2023GL103909 (2023).
- [62] O. Zlydenko, G. Elidan, A. Hassidim, D. Kukliansky, Y. Matias, B. Meade, A. Molchanov, S. Nevo, and Y. Bar-Sinai, A neural encoder for earthquake rate forecasting, *Scientific Reports* **13**, 12350 (2023).
- [63] D. W. Scott, *Multivariate Density Estimation*, 2nd ed. (Wiley, 2015).
- [64] P. Virtanen, R. Gommers, T. E. Oliphant, M. Haberland, T. Reddy, D. Cournapeau, E. Burovski, P. Peterson, W. Weckesser, J. Bright, S. J. van der Walt, M. Brett, J. Wilson, K. J. Millman, N. Mayorov, A. R. J. Nelson, E. Jones, R. Kern, E. Larson, C. J. Carey, Í. Polat, Y. Feng, E. W. Moore, J. VanderPlas, D. Laxalde, J. Perktold, R. Cimrman, I. Henriksen, E. A. Quintero, C. R. Harris, A. M. Archibald, A. H. Ribeiro, F. Pedregosa, and P. van Mulbregt, SciPy 1.0: Fundamental algorithms for scientific computing in Python, *Nature Methods* **17**, 261 (2020).

Extended Material for:  
 “Do earthquakes “know” how big they will be? a neural-net aided study”

Model	$\mathcal{L}$			$\mathcal{L}$ temporally conditioned			$\mathcal{L}$ spatially conditioned		
	Southern California	New Zealand	Japan	Southern California	New Zealand	Japan	Southern California	New Zealand	Japan
MAGNET	<b>0.28</b>	<b>0.37</b>	<b>0.62</b>	<b>0.25</b>	0.29	<b>0.60</b>	<b>0.27</b>	<b>0.31</b>	<b>0.47</b>
train set GR	0.37	0.64	0.74	0.28	0.46	0.70	0.36	0.41	0.51
test set GR	0.34	0.58	0.75	0.26	0.44	0.71	0.33	0.39	0.50
last 300 events GR	0.33	0.54	0.73	0.28	0.45	0.70	0.32	0.38	0.51
last 10 days GR	0.36	0.55	0.73	0.31	0.46	0.70	0.34	0.39	0.52
last 100 days GR	0.33	0.56	0.73	0.28	0.45	0.70	0.32	0.39	0.53
last 1000 days GR	0.33	0.57	0.74	0.27	0.45	0.70	0.32	0.40	0.53
train sets spatially varying GR	1.41	0.38	0.67	1.18	<b>0.19</b>	0.62	1.28	0.42	0.51
KDE of last 300 events	2.67	1.47	1.76	1.99	0.83	1.31	1.47	0.45	0.58
KDE of last 50 events	3.09	1.61	1.88	2.52	1.04	1.36	1.44	0.51	0.66

TABLE II. Mean score,  $\mathcal{L}$ , for all tested benchmarks.  $\mathcal{L}$  is computed by Eq. 1. Lower score indicates a better magnitude predictor, best score in column is indicated in bold. First 3 columns display scores for the raw calculation of  $\mathcal{L}$ , middle and right column triplets display the scores for the temporally and spatially conditioned  $\mathcal{L}$  scores, respectively.



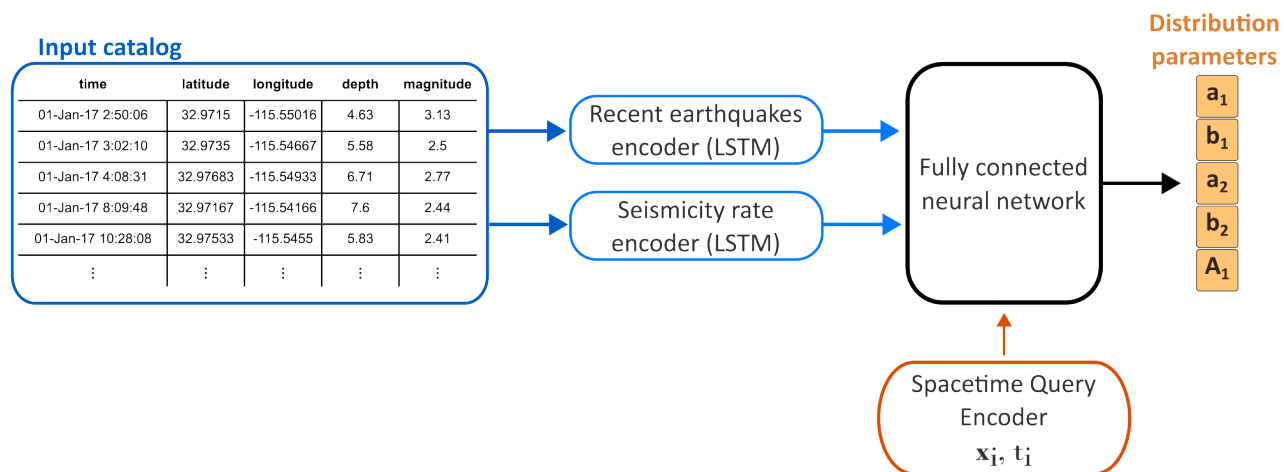


FIG. 5. **MAGNET architecture.** Described in detail in the methods section.

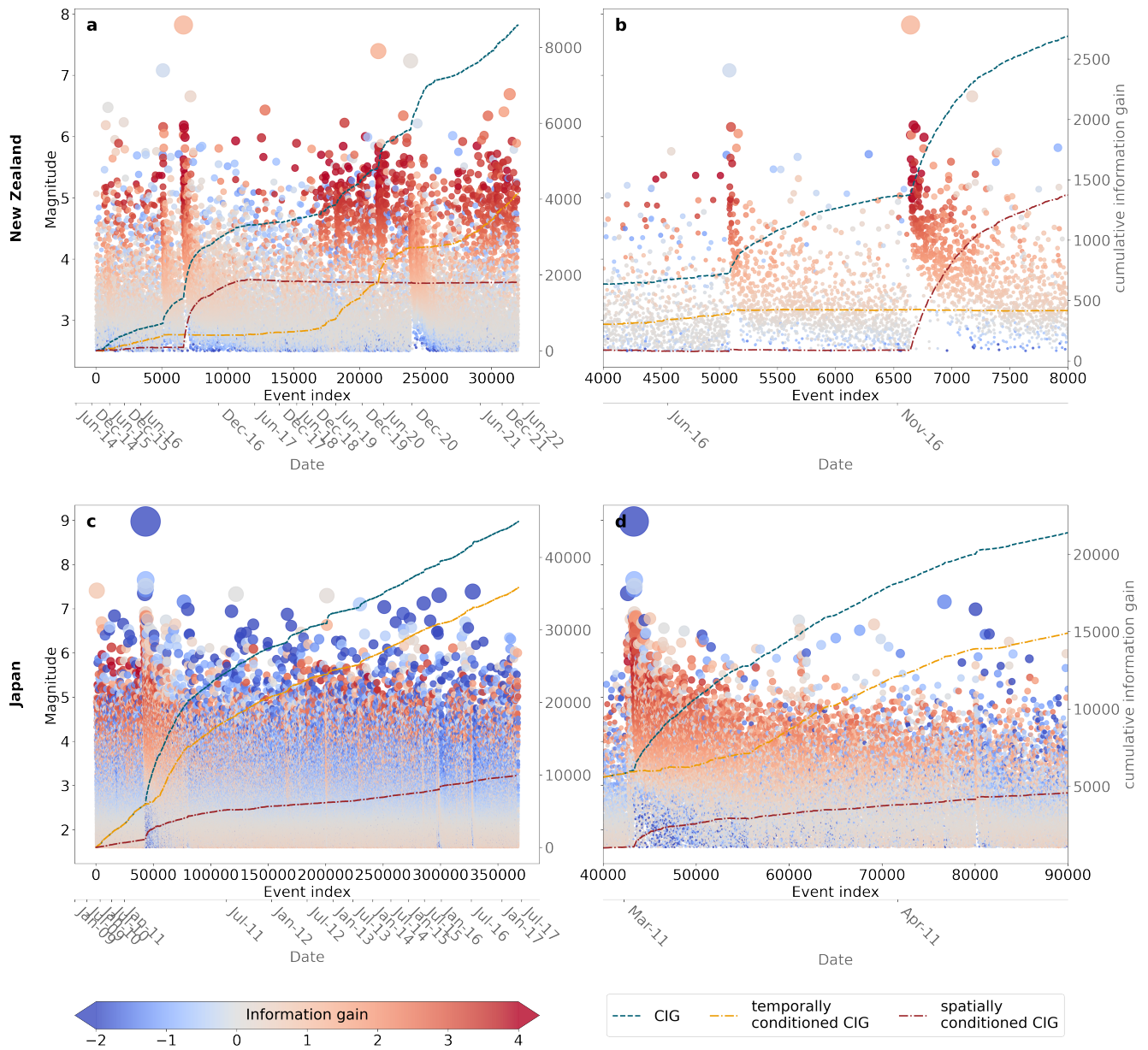


FIG. 6. **Information gain of MAGNET over the benchmark, New Zealand and Japan data sets.** Scattered dots indicate magnitude at event index, colored by the information gain per event. **a** Entire test set of New Zealand and a selected time span **(b)** focusing on the 2016 Te Araroa earthquake and the 2016 Kaikōura earthquake. **c** The entire Japan data set and a focused time span **d** of the 2011 Tōhoku earthquake and some of its aftershocks.

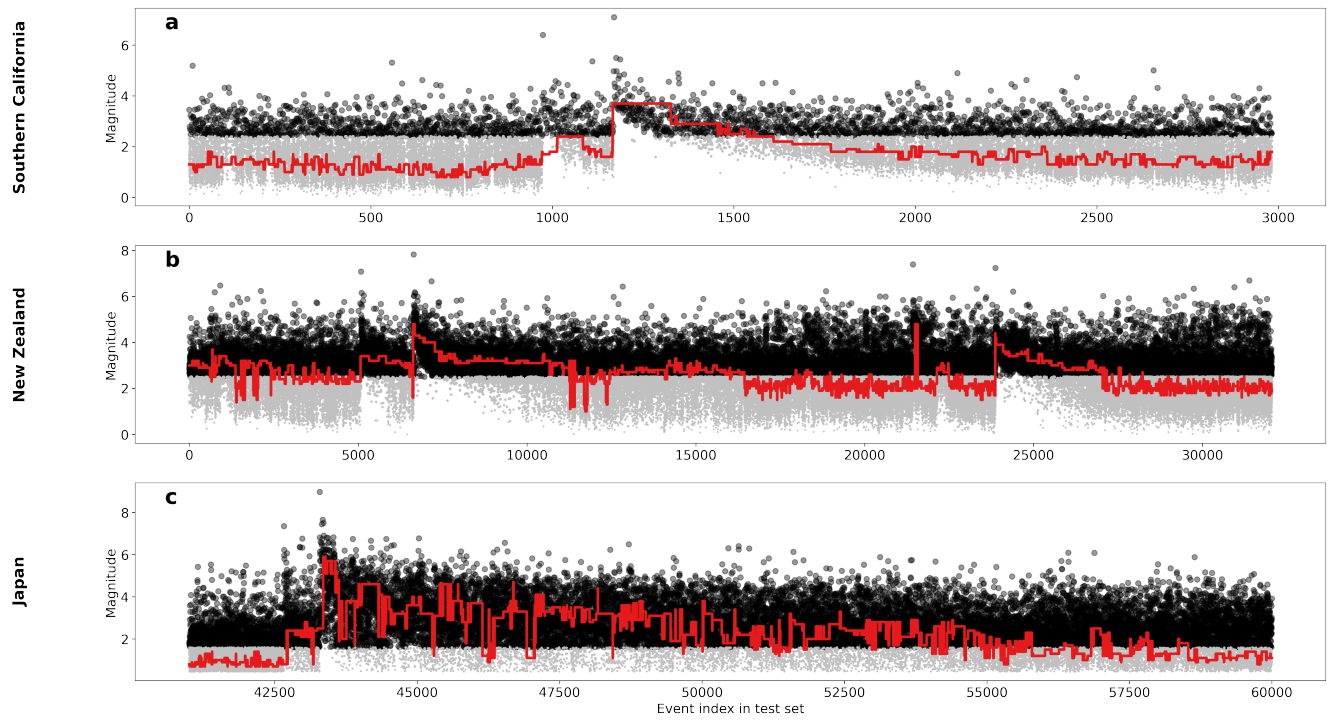


FIG. 7. **Temporal Incompleteness for test sets of all regions examined.** Calculated temporal incompleteness for test sets is presented in red, superimposed over the events above (black, included in model evaluation) and below (grey) the completeness magnitude of the train set,  $m_c^{(train)}$ . Events are plotted by the index of their appearance in the test set. Data for Japan (c) is displayed only near the 2011 Tōhoku earthquake to reduce data density and enhance clarity of the figure.

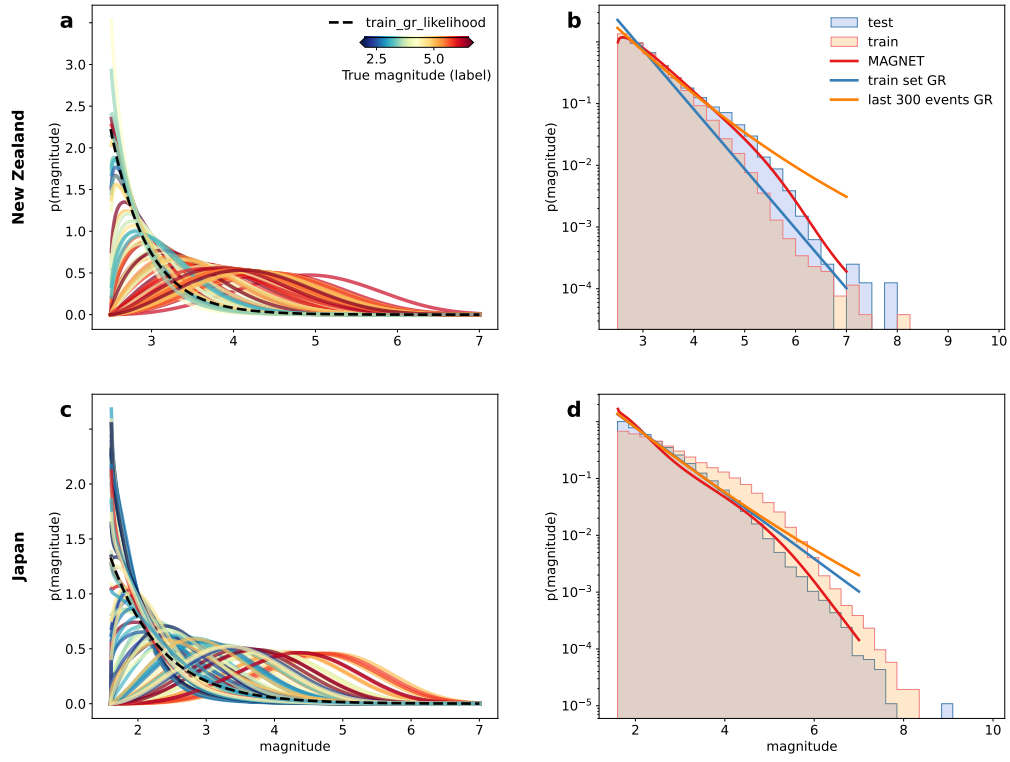


FIG. 8. **MAGNET's output for Japan and New Zealand data sets.** **a (c)**, PDFs produced by MAGNET for 100 randomly sampled events from the test set of the New Zealand (Japan) data set, with the train set's Gutenberg-Richter distribution superimposed (dashed black line). The true magnitude label, i.e. the true magnitude of the event in query, is indicated by the color, interpreted by the colorbar in **a**. **b (d)**, Marginal magnitude distribution, i.e. stationary  $p(m)$ , for the New Zealand (Japan) data set. Histograms of the train and test sets are presented in orange and blue respectively.



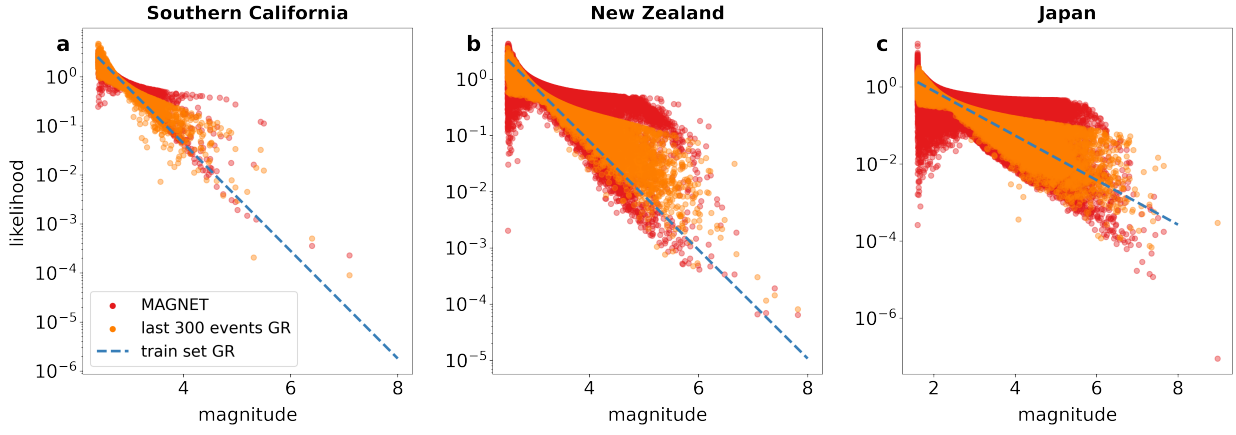


FIG. 9. **Log-likelihood of the true magnitude,  $\ell_i$ .** The likelihood for the true magnitude label of the test set for each data set,  $\ell_i = \log(p_{\mathbf{x}_i, t_i}(m_i))$ , as defined in main text.  $\ell_i$  values of MAGNET and the last 300 events benchmark are shown in red and orange respectively. The blue dashed line indicates the values that the GR benchmark would obtain. In this representation, a higher value indicates a better score for an individual event. Both MAGNET and 300 last events benchmark to be well above the GR performance. It can be seen that for all regions MAGNET spreads the likelihoods wider, and specifically clearly outperforms the 300 last events benchmark in a significant portion of events.

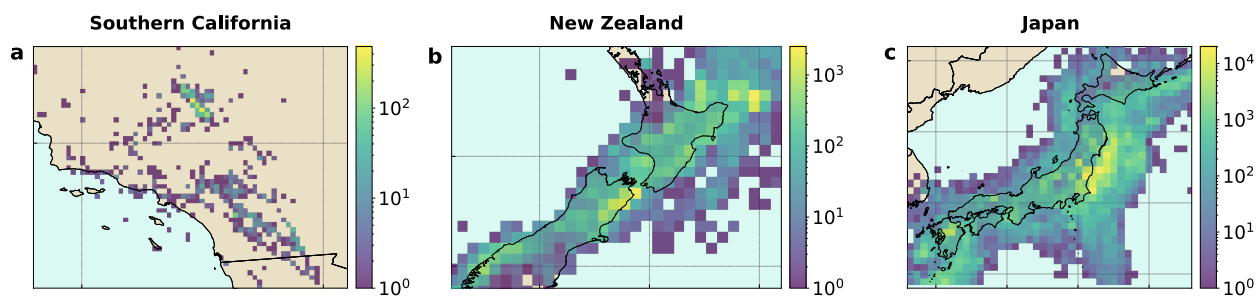


FIG. 10. **Event count in examined regions.** Number of events per bin is indicated in the adjacent color bar per inset. Bin divisions are identical to those presented in Figures 4e-g.